A&A 502, 705–709 (2009)
DOI: 10.1051/0004-6361/200811039

Astronomy & Astrophysics

Optimised data reduction for the AMBER/VLTI instrument⋆

A. Chelli, O. Hernandez Utrera, and G. Duvert

Laboratoire d'Astrophysique de Grenoble and Mariotti Center, UMR 5571 Université Joseph Fourier/CNRS, BP 53, 38041 Grenoble Cedex 9, France
e-mail: Alain.Chelli@obs.ujf-grenoble.fr

Received 25 September 2008 / Accepted 02 April 2009

ABSTRACT

Context. The signal processing of multi-aperture monomode interferometers using multiaxial recombination, such as AMBER/VLTI, makes use of the modeling of the fringes in the image space called the "P2VM method". This method was only validated on simulated data.
Aims. We aim to validate the P2VM method on-sky, and to use the knowledge acquired during more than three years of use of the instrument to provide improved data processing algorithms.
Methods. We compare the on-sky results of the P2VM algorithm with those provided by the standard, well known, and robust Fourier method.
Results. We first prove that the current implementation of the P2VM method used in the AMBER data reduction is biased for intermediate and low flux measurements. We determine the physical origin of these biases, then modify the data model accordingly, and introduce an improved noise model. We demonstrate that the P2VM method, together with the more realistic data and noise models, give results that are now in accordance with those provided by the Fourier method.

Key words. methods: data analysis – instrumentation: interferometers

1. Introduction

AMBER is the near infrared (1000–2500 nm) multiaxial beam combiner of the VLTI. It provides spatially filtered and spectrally dispersed visibilities for three simultaneous baselines and a phase closure (Petrov et al. 2007). AMBER data processing involves the modeling of the interferograms in the image space based on an internal calibration of the instrument. Chelli (2000) and Tatulli et al. (2007) showed that for the multiaxial recombination mode, there exists a linear relationship between the pixels of the interferogram and the instantaneous complex visibilities, and introduced the concept of the Pixel-to-Visibility Matrix (P2VM). This concept is not specific to the AMBER instrument and may be applied to extract the coherent fluxes from any monomode interferometer with multiaxial recombination.

Even though AMBER has been used extensively for three years and has produced numerous scientific results (see A&A special issue 464, N°1, 2007), the P2VM concept itself has never been validated on real data. The main goal of this paper is to perform this validation and to use the insights into the instrument gained during commissioning runs to improve the data and noise models. We validate the P2VM approach by comparing its results with those obtained from the well known and standard Fourier processing.

Section 2 briefly describes the P2VM algorithm as implemented today and presents a model of the internal calibrations used to measure the P2VM. In Sect. 3 we compare visibilities obtained with the present implementation of the P2VM method with those derived from a standard Fourier analysis. In Sect. 4 we present realistic data and noise models tailored for the AMBER instrument. The P2VM approach, using our data and noise models, is then validated in Sect. 5.

2. Amber data processing

2.1. Amber spatial recombination

The optical setup of AMBER, described in Robbe-Dubois et al. (2007), provides three photometric beams and one interferometric beam, which are formed along a line of the detector and then are spectrally dispersed along its columns. To increase the sensitivity, the conceptors of the instrument chose to minimize the number of pixels used to sample the fringes of the interferogram. However, in the process, the spatial coding of the fringes becomes so tight that their Fourier peaks partially overlap. Thus, the processing of the AMBER data is based on a modeling, spectral channel by spectral channel, of each interferogram. This requires an accurate internal calibration of the instrument together with realistic data and noise models.

2.2. The P2VM approach

Each one-dimensional interferogram can be described by

$$i_k = P_{1k} + P_{2k} + P_{3k} + c_{1k}R_{12} - d_{1k}I_{12} + c_{2k}R_{13} - d_{2k}I_{13} + c_{3k}R_{23} - d_{3k}I_{23}, \quad (1)$$

where i_k represents the number of photoevents from pixel k (k = 1...32 at present) of the interferogram; P_{lk} ($l = 1, 2, 3$) is the photometric contribution from telescope l and pixel k; R_{ln} and I_{ln} ($ln = 12, 13, 23$) are the real and imaginary parts of the coherent flux from telescopes l and n. c_{lk} and d_{lk} ($l = 1, 2, 3$) are the 3 carrying waves of the interferogram (containing the fingerprint of the instrument).

⋆ Partially based on observations collected at the European Southern Observatory, Paranal, Chile, within the commisioning programme 60.A-9054(A).

The calibration needed to model the fringe patterns is performed with the help of an internal lamp, as frequently as the stability of the instrument requires. Firstly, it consists of 3 photometric calibrations, 1 beam opened and the 2 other closed, providing the ratio

$$v_{lk} = \frac{P_{lk}}{K_l}, \quad (l = 1, 2, 3), \tag{2}$$

where K_l is the total number of photoevents from photometric beam l. The knowledge of the v_{lk} coefficients allows us to estimate the continuum and then to produce continuum corrected interferograms m_k as

$$\begin{aligned} m_k &= i_k - v_{1k}K_1 - v_{2k}K_2 - v_{3k}K_3 \\ &= c_{1k}R_{12} - d_{1k}I_{12} + c_{2k}R_{13} - d_{2k}I_{13} + c_{3k}R_{23} - d_{3k}I_{23}. \end{aligned} \tag{3}$$

Secondly, 6 interferometric calibrations are performed, 2 beams opened at a time, each with 2 measurements, shifted by $\pi/2$. These measurements provide the carrying waves c_{lk} and d_{lk}. Tatulli et al. (2007) showed that the relationship between the measured m_k on an interferogram and the complex coherent flux (R_{ln},I_{ln}) is given by

$$\begin{pmatrix} m_1 \\ \vdots \\ m_k \\ \vdots \end{pmatrix} = \mathrm{V2PM} \begin{pmatrix} \vdots \\ R_{ln} \\ \vdots \\ I_{ln} \\ \vdots \end{pmatrix}, \tag{4}$$

where V2PM is the "visibility to pixel" matrix. The knowledge of the carrying waves allows us to estimate the coherent fluxes from a linear least square fit of each spectral channel, by minimizing the quantity

$$\chi^2 = \sum_k \left(\frac{m_k - c_{1k}R_{12} + d_{1k}I_{12} - c_{2k}R_{13} + d_{2k}I_{13} - c_{3k}R_{23} + d_{3k}I_{23}}{\sigma_k} \right)^2, \tag{5}$$

where σ_k is the error of m_k. In practice, the coherent fluxes are obtained by multiplying the vector of components $\{m_k\}$ by the "pixel to visibility" matrix P2VM

$$\mathrm{P2VM} = [\mathrm{V2PM}^T\, C_\mathrm{M}^{-1}\, \mathrm{V2PM}]^{-1}\, \mathrm{V2PM}^T\, C_\mathrm{M}^{-1}, \tag{6}$$

where C_M is the covariance matrix of the measurements m_k, initially assumed diagonal in the current implementation of the AMBER data processing (hereafter "standard P2VM"), and ^{T} is the transposition operator.

2.3. AMBER interferometric observables

The AMBER intrument provides square visibilities, differential phases (see Sect. 4.4) and closure phases. The square visibilities are derived from the coherent fluxes by

$$V_{ln}^2 = \frac{\left\langle R_{ln}^2 + I_{ln}^2 - \epsilon_{R_{ln}}^2 - \epsilon_{I_{ln}}^2 \right\rangle}{4 \left\langle K_l K_n \right\rangle \sum_k v_{lk} v_{nk}}, \quad (ln = 12, 13, 23), \tag{7}$$

where $\epsilon_{R_{ln}}$ and $\epsilon_{I_{ln}}$ are the errors on the real and the imaginary part of the coherent flux, and $\langle\rangle$ denotes the ensemble average over the set of interferograms.

The phase closure is the phase of the average bispectrum B_{123} defined as

$$B_{123} = \langle (R_{12} + jI_{12}) \times (R_{23} + jI_{23}) \times (R_{13} - jI_{13}) \rangle\,. \tag{8}$$

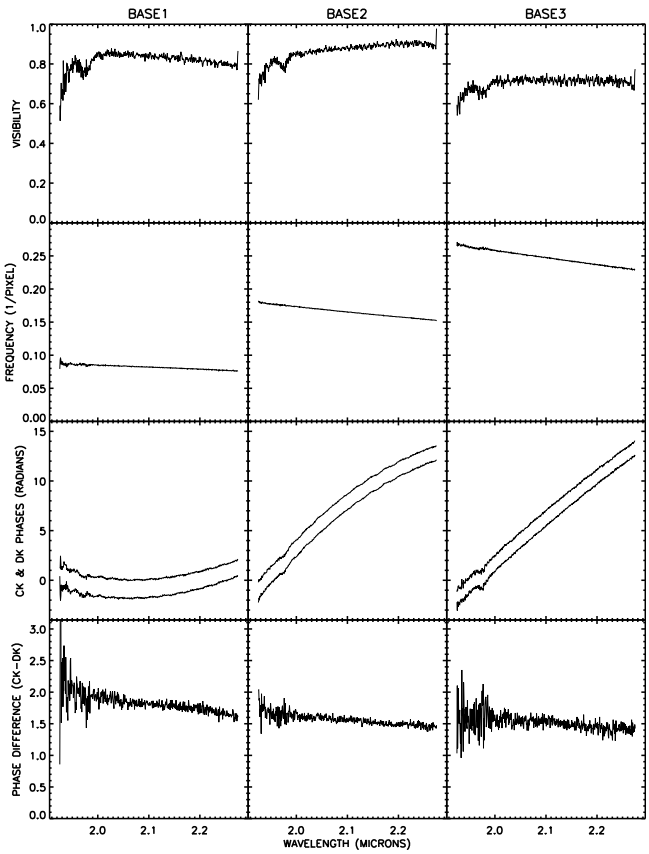

Fig. 1. Characterization of a medium resolution (R = 1500) P2VM with 3 telescopes in the K band. *From top to bottom*, as a function of the wavelength: visibility, frequency (in pixel^{-1}), phases of the c_k and d_k (radians), and their difference.

2.4. P2VM characterization

The initial design of AMBER required only that the computation of the P2VM could be done with a sufficiently good signal-to-noise ratio. This was easily obtained given the flux of the calibration lamp. Similarly, the knowledge of the intrinsic visibility of the calibration lamp on the three spatial frequencies, its differential phase and phase closure, all implicitly contained in the c_{lk} and d_{lk} elements of Eq. (3), was not required. Indeed, their imprint (through the P2VM values) on the raw visibilities cancels out during the calibration of the object's visibility by the visibility of a calibrator, *obtained with the same P2VM*.

To gain better insight into the parameters used in building the P2VM, we modeled the carrying waves in terms of visibilities, frequencies and phases. We show in Fig. 1 the results for a medium resolution (R = 1500) P2VM observation. At the top, we have plotted the 3 system visibilities (between the calibration lamp and the detector) as a function of the wavelength; below are the three spatial frequencies of the fringes expressed in pixel^{-1}; next to them, the phases of the carrying waves and then their difference are given. The phases of the carrying waves vary by more than 10 radians (i.e., 2λ) along the spectrum, which is negligible compared to the coherence length of 1500λ at medium resolution. Before processing, the experimental carrying waves are corrected for the system visibilities and their phase difference is set to $\pi/2$.

3. Comparison between AMBER and Fourier estimators

3.1. P2VM vs. Fourier methods

To assess the robustness of the present AMBER data processing, we made an extensive comparison between the P2VM visibilities and those of the classical Fourier method. This approach is legitimate since the Fourier method has been long proven to be robust. Indeed, it allows us to perform a direct estimate of the mean visibility from the average power spectrum without any a priori, unlike the P2VM method, where one must extract the coherent fluxes by modeling each interferogram separately to estimate the mean visibility. This in turn requires precise data and noise models.

The Fourier method can be applied only if the fringe peaks in the Fourier plane do not overlap. For AMBER, this condition is not met when used with three telescopes. In consequence, we performed the comparison on commissioning data obtained with two telescopes (giving a single fringe peak in the Fourier plane). The Fourier square visibilities are computed as the ratio between the energy W of the averaged interferometric peak power spectrum and the average of the photometric fluxes product, namely

$$V_{12}^2 = \frac{W}{\langle K_1 K_2 \rangle \sum_k v_{1k} v_{2k}} \cdot \quad (9)$$

We estimated W by fitting the averaged interferometric peak power spectrum with the sum of a Gaussian (for the peak) and a 2nd degree polynomial (for the background).

3.2. Results

The comparison was performed on a set of 90 observations obtained in medium resolution mode on July 17th 2006, during AMBER Commissioning 4 (COM4) with 2 auxiliary telescopes and 2 different baselines of 32 and 64 m. The observed sample was selected to cover a wide range of observational conditions in terms of zenithal distance, magnitudes, intrinsic visibilities and integration time (ranging from 0.02 s to 0.16 s).

The visibilities, computed with both methods and averaged in wavelength, are represented in Fig. 2 as a function of the average flux per interferogram. For high fluxes, the two approaches provide, within the noise, the same visibilities. However, they begin to deviate from each other at fluxes below a few hundred photoevents per interferogram. Below this limit, the current implementation of the P2VM method provides visibilities systematically higher than the Fourier values, and even visibilities larger than 1 for small S/N interferograms, with a difference increasing as the flux decreases.

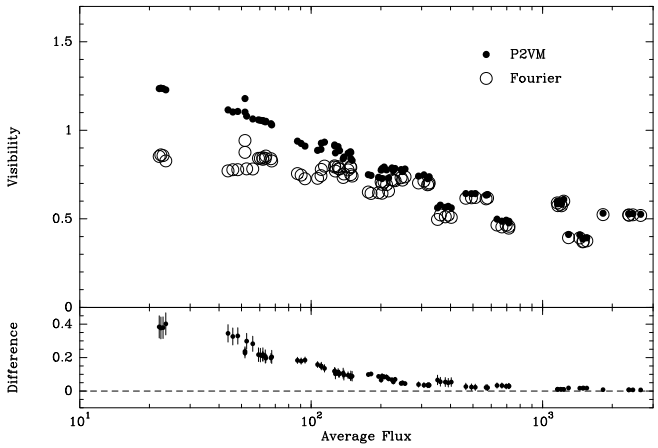

Fig. 2. *Top*: comparison of the visibilities, averaged in wavelength, obtained with the current implementation of the P2VM method (black dots) and the classical Fourier method (circles). *Bottom*: visibility difference between the methods; the error bars are those of the P2VM.

4. An improved AMBER data processing

We have been able to trace back the origin of the discrepancies highlighted in the previous section, by making an end-to-end critical examination of the calibration process of AMBER. We found two critical issues: 1) an incomplete data model overlooking both the presence of stray light and optical ghosts in the spectrograph and non-linearity effects in the detector at low fluxes; 2) a too simplistic noise model.

4.1. Dealing with stray light during the P2VM calibration

There is a variable amount of stray light in the spectrograph due to optical misalignments, imperfect baffling and reflexions in the beam separator. These optical ghosts introduce some amount of light in the supposedly closed beams during the calibration process. This light from a "closed" beam is by design distributed to the interferometric beam during the calibration process. Hence the calculation of the v_{lk} coefficients should consider all the beams, as follows

$$P_{lk} = v_{1k} K_1 + v_{2k} K_2 + v_{3k} K_3, \quad (l = 1, 2, 3)\,. \quad (10)$$

The 3 photometric calibrations provide a set of 3 equations with 3 unknowns that are to be solved pixel by pixel.

This correction in the value of the v_{lk} is critical, however it will not compensate for the effect of stray light that would leak directly onto the camera at the location where the interferometric beam is imaged. When such stray light is present, its effect will be largely compensated for by the second correction we describe below.

4.2. Continuum regularization

It is mandatory, especially at low fluxes, to have a good estimate of the continuum in order to obtain the true continuum-corrected interferogram. Since the v_{lk} are calibrated at high flux, their value at low flux may be different in the presence of detector non-linearity, and the continuum correction will be inaccurate. To prevent any non-linear effect, we introduce a new parameter, A, which forces our data model to match the continuum by minimizing the quantity

$$\chi^2 = \sum_k \left(\frac{V_k}{\sigma_k} \right)^2 , \quad (11)$$

with

$$\begin{aligned} V_k &= i_k - A \times \left[v_{1k} K_1 + v_{2k} K_2 + v_{3k} K_3 \right] \\ &+ c_{1k} R_{12} - d_{1k} I_{12} + c_{2k} R_{13} - d_{2k} I_{13} + c_{3k} R_{23} - d_{3k} I_{23}\,. \end{aligned} \quad (12)$$

The parameter A should be evaluated line by line on the *mean interferogram* via a 7 parameter fit, A and the 3 complex coherent fluxes. Once estimated, A is fixed and becomes a multiplicative factor for the v_{lk}. Then the coherent fluxes can be extracted frame by frame via the 6 parameter standard adjustment.

4.3. Improving the noise model

The modeling of the continuum with the photometric fluxes introduces correlations between pixels that need to be taken into account, especially at low fluxes. The quantity to be minimized becomes

$$\chi^2 = V^T \times C^{-1} \times V, \tag{13}$$

where V is the vector of components $\{V_k\}$ and C is the covariance matrix defined by its elements

$$\begin{aligned} C_{kl} &= A^2 \left[v_{1k} v_{1l} \sigma^2(K_1) + v_{2k} v_{2l} \sigma^2(K_2) + v_{3k} v_{3l} \sigma^2(K_3) \right], \ (k \neq l) \\ C_{kk} &= \sigma^2(i_k) + A^2 \left[v_{1k}^2 \sigma^2(K_1) + v_{2k}^2 \sigma^2(K_2) + v_{3k}^2 \sigma^2(K_3) \right]. \end{aligned} \tag{14}$$

There are three sources of noise: the photon noise from the observed object, that of the background (both described by Poisson statistics) and the detector readout noise. The quadratic sum $\sigma_{\rm d}^2$ of the detector readout noise and the background photon noise is estimated pixel by pixel, on the set of dark or (preferably) sky frames. $\sigma_{\rm d}^2$ is approximated by the variance of the pixel value along the frames. The variances $\sigma^2(i_k)$ and $\sigma^2(K_l)$ are then given by

$$\begin{aligned} \sigma^2(i_k) &\approx E(K_{ik}) + \sigma_{d_{ik}}^2 \\ \sigma^2(K_l) &\approx E(K_l) + \sum_k \sigma_{d_k}^2, \quad (l = 1, 2, 3) \end{aligned} \tag{15}$$

where K_{ik} is the number of photoevents from the object at pixel k of the interferometric beam, and E is the expected value. As these variances are used in the P2VM computation through the use of the generalized inverse, they must be estimated with care. $E(K_l)$ may be approximated by the instantaneous value K_l, but not $E(K_{ik})$, for at low fluxes it would lead to noisy and thus unstable covariance matrices. Instead, we use the shape of the average interferogram to scale the instantaneous object photon noise, as follows

$$E(K_{ik}) \approx \frac{\langle K_{ik} \rangle}{\sum_k \langle K_{ik} \rangle} \times \sum_k K_{ik}. \tag{16}$$

With this new approach, the covariance matrix should be computed and inverted spectral channel by spectral channel and frame by frame.

4.4. A robust differential phase estimator

We introduce here a robust method to estimate the differential phase $\phi_{\rm d}(\lambda)$, namely the phase of the object spectrum as a function of the wavelength. For this purpose, one needs to evaluate the optical path difference (OPD), interferogram by interferogram. In the current implementation of the AMBER data reduction (Tatulli et al. 2007), the OPD is retrieved from the phase $\phi(\lambda)$ of the interferogram itself. Since $\phi(\lambda)$ is given by

$$\phi(\lambda) = \phi_o(\lambda) + 2\pi\delta/\lambda, \tag{17}$$

where ϕ_o is the phase of the object spectrum and δ is the OPD, the OPD evaluation should be performed using only the spectral regions for which the object phase $\phi_o(\lambda)$ is assumed to be zero.

To overcome this difficulty we propose to compute the cross spectrum between the coherent flux of each interferogram and that of a reference interferogram at the same wavelength. Let C_λ^k and C_λ^r be the coherent fluxes at wavelength λ, from the kth interferogram and a chosen reference interferogram r, the phase of the cross-spectrum $C_\lambda^k \times C_\lambda^{r*}$ is given by

$$\Delta\phi(\lambda) = 2\pi(\delta_k - \delta_r)/\lambda. \tag{18}$$

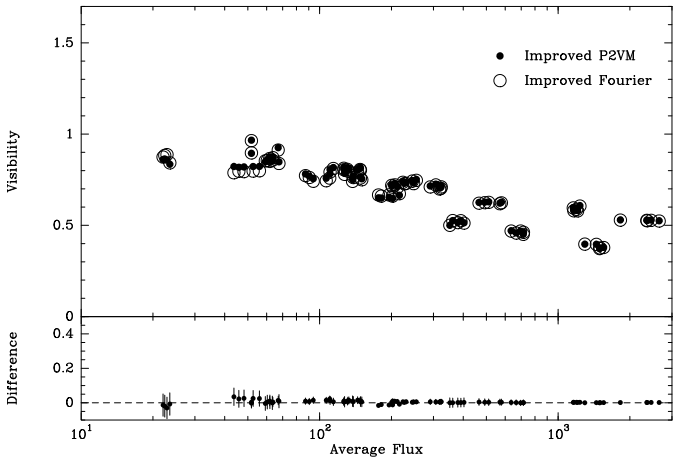

Fig. 3. *Top*: comparison of the visibilities, averaged in wavelength, obtained with the improved P2VM method (black dots) and the improved Fourier method (circles). *Bottom*: visibility difference between the methods; the error bars are those of the P2VM. The two approaches now provide fully consistent results at any range of flux.

The phase of the cross spectrum has a real differential property in the sense that the unknown object phase has been eliminated. Thus, the result can now be properly modeled, using the full spectral coverage, to estimate the OPD difference $\delta_k - \delta_r$, interferogram by interferogram. From here, the differential phase $\phi_{\rm d}(\lambda)$ can be extracted from the average OPD-corrected coherent fluxes, as follows

$$\phi_{\rm d}(\lambda) = \arg\left\{ \left\langle C_\lambda^k \times {\rm e}^{-2i\pi(\delta_k - \delta_r)/\lambda} \right\rangle_k \right\}. \tag{19}$$

5. Validation of the method

5.1. Comparison between the Fourier estimator and the improved P2VM estimator

We have implemented the new data and noise models in a new version of the AMBER data reduction software (hereafter "improved P2VM"). We then did the comparison with the Fourier processing on COM4 data like in Sect. 3. Since the Fourier method also needs a good estimate of the photometries, we must apply the same continuum regularization using the parameter A (hereafter "improved Fourier"), that is

$$V_{12}^2 = \frac{W}{A^2 \langle K_1 K_2 \rangle \sum_k v_{1k} v_{2k}}. \tag{20}$$

The visibilities derived from the improved P2VM and the improved Fourier method are plotted in Fig. 3, as a function of the average flux per interferogram. Clearly, the more realistic data and noise models now provide a very good agreement between the two processes in any range of fluxes. Indeed, the scatter of the visibility difference is 1% below 200 photoevents per interferogram, and only 0.5% for larger fluxes. In addition, it seems that the improved P2VM visibilities present less scatter at low flux than the Fourier visibilities. This could be an indication that the P2VM method brings more accurate results than the Fourier method, as suggested by Le Bouquin & Tatulli (2006).

We also investigate the impact of the new processing on the visibility as a function of wavelength. Figure 4 shows the spectral distribution of the visibility of a bright source, as estimated by the "standard" and "improved" methods (the latter

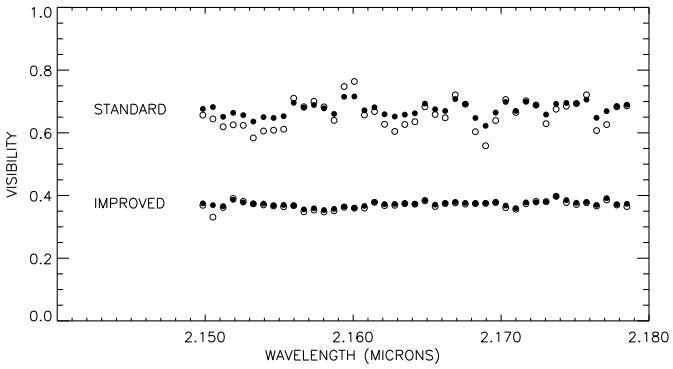

Fig. 4. *Top*: standard P2VM (open circles) and Fourier (black dots) visibilities of a bright source as a function of wavelength. The visibilities are fully consistent, but possess large structures. *Below*, the visibilities (shifted down by 0.3 for clarity) derived from the improved P2VM and Fourier approaches: the structures have nearly completely been removed.

being shifted down by 0.3 for clarity). One sees at the top of the figure that the standard P2VM and Fourier visibilities are compatible (the source was bright), but exhibit large, perhaps structured, variations along the spectrum. Below, the improved visibilities: not only do they agree, but the structures have been nearly completely removed. Hence, the new data processing not only produces compatible results between the P2VM and the Fourier approaches, but also allows us to regularize the Fourier visibilities by providing more realistic photometric fluxes.

5.2. Stability of AMBER/VLTI

Now that we have removed obvious biases in the AMBER visibility measurements, we can estimate the stability of the VLTI with AMBER as a by-product of this study. This is customarily done by examining the dispersion of the visibility on one or more calibrators during the night, taking into account their instrinsic visibility change with the projected baseline length if, as is the case here, some of them are resolved.

Figure 5 shows the visibility as a function of time for the calibrators of the COM4 dataset observed with integration times of 20 and 80 ms. The dataset covers 3.5 mag in brightness and the stars are scattered on the celestial sphere. One sees that eventhough for each calibrator the visibilities decrease with integration time, the transfer function for the night (broken lines) keeps the same shape. For the 6 h span presented here the visibilities calibrated by their respective transfer function present a dispersion of ~4.5%.

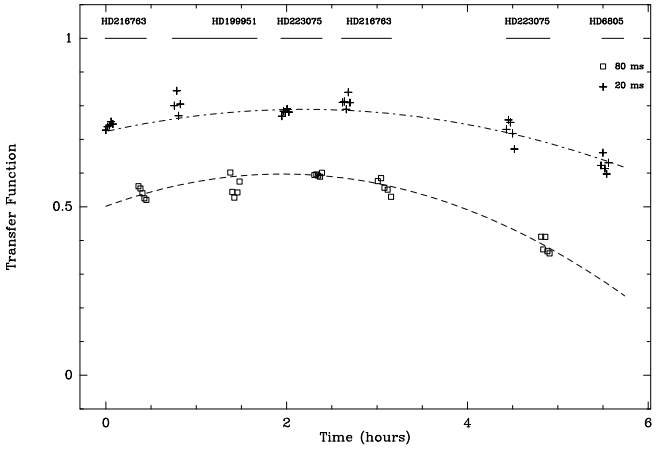

Fig. 5. Transfer function of one COM4 night, obtained with the improved AMBER data reduction software, on the same dataset as in Fig. 3. The symbols differentiate the two integration times used, 20 ms and 80 ms. The dotted and dashed lines are the best second-degree polynomial that would interpolate the transfer function of the night for each integration time.

6. Conclusion

To validate on-sky the P2VM approach used to process AMBER data, we compared the visibilities obtained with this method against those derived from a standard Fourier analysis. We found large discrepancies between the two methods at intermediate and low fluxes. We showed that the data model used in the current implementation of the AMBER data reduction is inadequate due to an incorrect photometry estimate. We propose solutions to correct this effect and we introduce a more realistic noise model. Using these improved data and noise models, we now find a complete agreement between the P2VM and Fourier approaches, thus validating the P2VM concept. A new version of the AMBER Data Reduction Sofware including the work described here, will be issued shortly by the Jean-Marie Mariotti Centre[1].

Acknowledgements. We thank F. Malbet, P. Kern, E. Tatulli and O. Absil for their useful comments and support of this work. We also thank two anonymous referees whose comments helped us to improve the clarity of this paper.

References

Chelli, A. 2000, AMBER Data Processing, Amber Memorandum AMB-IGR-018, Tech. Rep.
Le Bouquin, J.-B., & Tatulli, E. 2006, MNRAS, 372, 639
Petrov, R. G., Malbet, F., Weigelt, G., et al. 2007, A&A, 464, 1
Robbe-Dubois, S., Lagarde, S., Petrov, R. G., et al. 2007, A&A, 464, 13
Tatulli, E., Millour, F., Chelli, A., et al. 2007, A&A, 464, 29

[1] See http://www.mariotti.fr